Two-dimensional model of orificed micro-hollow cathode discharge for space application

D. Levko,[1] Ya. E. Krasik,[1] V. Vekselman,[1] and I. Haber[2]
[1]*Department of Physics, Technion, 32000 Haifa, Israel*
[2]*University of Maryland, College Park, Maryland 20742-3511, USA*

(Received 27 April 2013; accepted 4 August 2013; published online 21 August 2013)

In this paper, we describe results of self-consistent two-dimensional (x-z) particle-in-cell simulations, with a Monte Carlo collision model, of an orificed micro-hollow cathode operating in a planar diode geometry. The model includes thermionic electron emission with Schottky effect, secondary electron emission due to cathode bombardment by the plasma ions, several different collision processes, and a non-uniform xenon background gas density in the cathode-anode gap. Simulated results showing behavior of the plasma density, potential distribution, and energy flux towards the hollow cathode and orifice walls, are discussed. In addition, results of simulations showing the effect of different *Xe* gas pressures, orifice size, and cathode voltage, on operation of the micro-hollow cathode are presented. © *2013 AIP Publishing LLC*.
[http://dx.doi.org/10.1063/1.4818969]

I. INTRODUCTION

Currently, hollow cathodes (HC) are widely used in spectral lamps,[1] laser applications,[2] surface modification,[3] electric propulsion,[4–9] etc. Earlier research[10,11] has shown HC behavior, where at a given applied voltage, for certain cathode geometries increased current density is observed compared with a planar anode-cathode geometry. In order to explain this phenomenon different mechanisms have been proposed, such as, photon induced secondary emission, electron pendulum motion in the potential well formed by the plasma positively charged with respect to the cathode walls, ionization in the cathode fall, and ion induced secondary electron emission. Recent research (see, for instance, Ref. 4) has shown that depending on initial conditions (HC geometry, gas pressure, etc.) different phenomena contribute to the HC effect. For instance, if the gas pressure inside the HC is small and electron mean free path exceeds the inner diameter of HC, the effect of electron pendulum motion inside the HC becomes important phenomenon in the HC discharge.[12,13] According to this effect electrons emitted by the cathode and generated in the cathode sheath experience oscillations in the potential well formed by a positively charged plasma and which depth exceeds the ionization potential of the propellant gas. Thus, these oscillating electrons have enough energy to ionize the gas thus keeping HC discharge. At the larger gas pressure, when the electron mean free path becomes smaller than the diameter of the HC, the discharge is supported mainly by electrons emitted from the cathode and accelerated in the cathode sheath.[4]

Thermionic HCs with an orifice plate (orificed HC) are widely used in electric thrusters,[4–9] where these cathodes can be considered as essential components, providing an efficient source of electrons for both propellant ionization and neutralization of the extracted ion beam. The comparative simplicity and small physical volume of the HC are attractive features for micro- or nano-satellite propulsion applications that require high specific impulse of ion propulsion. In general, the operation of the HC is complex and depends on many parameters, for instance, type and flow rate of gas, applied voltage, HC, and orifice dimensions, type of thermionic emitter, etc. Thus, an understanding of HC operation is important to providing support for its improved development. In the past decade, a significant number of research has been devoted to HC discharges (see Refs. 1–4, 10–30, and references therein). In order to describe the operation of the HC, global and one-dimensional models were developed (see, for instance, Refs. 4, 17, and 21). However, these models do not allow self-consistently calculation of the density, temperature, and potential of the plasma inside the cathode with thermionic emitter, including the effects occurring in the vicinity of the cathode orifice.

In order to obtain these parameters, self-consistently at least a two-dimensional (2D) model is required. Recently, several 2D models of HC discharge (see Refs. 12, 13, 15, 16, and 19–30) were developed. Though some of these models are capable of simulating the initiation process no such results have been reported in the literature. Boyd *et al.*[19] developed the hybrid model of the plasma plume of orificed HC, which has the inner diameter of 1 mm, length of 11 mm, and orifice plate diameter of 0.2 mm. In this model, electrons were described by fluid equations, while ions and neutrals were treated using a Particle-in-Cell (PIC) method with the plasma density and electron temperature at the HC exit as boundary conditions.

More sophisticated 2D fluid simulation models (see Refs. 22–30) were developed by Mikellides *et al.* for two orificed HCs, which have cathode diameters of 0.635 cm and 1.5 cm, length of 2.54 cm, orifice diameters of 0.1 cm, and 0.3 cm, and internal gas pressure of 7.88 Torr and 1.07 Torr. The first model[22–24] (IROrCa2D) is the 2D-axisymmetric time-independent fluid model, which was applied for studying the plasma parameters only inside the HC. This model solves the conservation equations for electrons and Xe^+ ions

fluids neglecting the inertia terms in the electron and ion momentum equations. The quasineutrality between electrons and singly charges ions Xe^+ is assumed, and sheaths near the cathode and orifice plate were not considered in this model. The electron temperature is obtained from the electron energy transport equation, which includes thermal diffusion, energy loses due to ionization, and the work done on the electrons by the electric field. Electron emission from the cathode is described by the Richardson-Dushman equation with the accounting for Schottky effect. The emitter temperature obtained from experimental data was taken as a boundary condition, and the orifice plate temperature was set equal to the peak emitter temperature. The neutral gas dynamics was considered in the model OrCa2D-I.[22] The neutral gas density was obtained from the neutral gas continuity equation and inside the HC the neutral gas viscous momentum equation was solved as well as inertia terms, and plasma plume regions were considered in this model. Both IROrCa2D and OrCa2D-I models used classical resistivity of low-ionized plasma.[31] The anomalous plasma resistivity calculated using the measured plasma parameters (plasma potential, electron density, electron temperature, and electron current density) was applied in OrCa2D-II[25] model in order to obtain better agreement with the experimental data. The heating of the HC and its cooling by radiation and thermal conduction was simulated in Ref. 27, where the temperature distribution along the cathode was obtained using as input parameters the electron and ion fluxes to the cathode surface from OrCa2D model. The model OrCa2D was updated with considering the keeper, which was considered with the floating potential in Ref. 30. The keeper plate temperature was set constant and equal to 500 °C. Thin-sheath boundary conditions were applied at the cathode wall boundaries, and the cathode wall temperature was taken from the experimental data.

The results of these simulation studies[22–30] showed that electrons are heated due to classical collisions almost in the entire HC volume, except vicinity of the orifice, where electrons are heated by electrostatic instabilities. The largest plasma density, $n_e \sim 10^{22}\,m^{-3}$ and temperature, $T_e \sim 2\,eV$, were found in the center of the orifice. Also, it was shown that in the HC operating with 25 A discharge current and low gas pressure, neutral gas dynamics is not significant. Opposite, in smaller cathodes operating at much higher pressures, both neutral gas dynamics and viscous effects were found to be important. Finally, it was shown that secondary electron emission does not have significant effect on operation of the HC with large discharge current. However, these fluid models did not account for kinetic effects that could occur in the cathode exterior due to deviations from the Maxwellian distribution function there. This could lead (among others) to an increase in the electron-neutral collision rate coefficients, which could lead to the overestimation/underestimation of the plasma parameters.

In order to study the HC discharge dynamics Crawford *et al.*[16] developed a PIC Monte Carlo Collision (PIC MCC) model. This model considers three kinds of super-particles (electron, ion, and neutral) which collide with each other (electron-neutral elastic and inelastic collisions, and ion-neutral elastic and charge exchange collisions) and thermionic emission of electrons. The HC considered in this model has both orifice and keeper. The main objective of these simulations was to study the parameters of neutral gas flow inside the HC and the plasma parameters reported in Ref. 16 did not reach the steady state values during 14 μs. During that time, the largest energy of electrons was obtained near the keeper and it was shown that the HC behaves like a choked nozzle.

In this paper, we describe the results of a self-consistent 2D PIC MCC model of the orificed micro-HC operating in the planar diode geometry at Xe gas pressure >50 Torr. This model, similar to the fluids models described in Refs. 22–30, also considers thermionic electron emission which accounts the Schottky effect, non-uniform Xe gas density in the cathode-anode gap and secondary electron emission due to cathode bombardment by the plasma ions. In fact, one can consider the present models as a simplified one as compare with significantly more sophisticated fluids models. Indeed, in the present form, this model does not consider processes related to the cathode temperature self-consistent distribution, neutrals are considered as a background gas, as well as this model considers orifice plate at the cathode potential and there is no keeper at floating potential. However, we can note an advantage of this simplified PIC model over fluid models[22–30] consisting in the absence of assumption of Maxwellian electron energy distribution function and accounting for the temporal evolution of ion energy distribution function, which in some cathodes (including the one studied here) can be non-Maxwellian. The simulation time which one requires to reach the steady-state solution of this PIC MCC model of micro-HC using common desktop computer is in the range of 2–3 days. Carried out simulation research using this model allowed to obtain the influence of gas pressure, orifice size, and cathode voltage on parameters of the micro-HC operation. Finally, the results of these simulations were compared with the results of 2D fluid models.[22–30]

II. NUMERICAL MODEL

An orificed micro-HC discharge was studied using the two-dimensional Cartesian module of the open-source WARP[32] PIC code, employing the code's multi-grid Poisson solver to obtain the self-consistent electrostatic fields. The cathode geometry is shown in Fig. 1. The model employed two space and two velocity (2D–2 V) components.

Each computational cycle with time step dt consists of the following steps:

(1) Electron emission from the surface of the HC emitter was described by the Richardson-Dushman[4] law with accounting for Schottky effect

$$J(x) = DT^2 \exp\left(\frac{-e\varphi_0}{kT}\right) \cdot \exp\left(\frac{e}{kT}\sqrt{\frac{eE_C(x)}{4\pi\varepsilon_0}}\right). \quad (1)$$

Here, the Schottky effect is accounted for by the second exponent containing the electric field $E_C(x)$ at the cathode surface. In Eq. (1), $D = 1.2 \times 10^6\,A{\cdot}m^{-2}K^{-2}$ is the

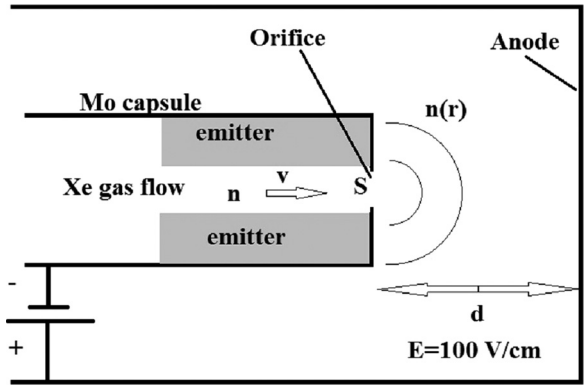

FIG. 1. Geometry of the orificed HC, which was used for modeling.

constant, which value is defined by the emitter material,[4] T is the temperature of the emitter, φ_0 is the emitter work function. The value of electric field $E_C(x)$ is calculated by solving the Poisson equation. In the model, the value $\varphi_0 \approx 1.5$ eV is taken from Ref. 4, and the gas temperature was assumed equal to the emitter temperature $T = 1500$ K. It is understood that, in general, the latter assumption is not valid, since the gas temperature could be significantly larger due to electron and neutral-ion charge exchange collisions. Also, due to the non-uniform plasma density distribution along the cathode, the gas temperature also has to be non-uniform.[4] These issues will be considered in the PIC model in our future simulations.

(2) Solution of the self-consistent electric field from the calculated charge densities, application of the self-consistent fields to change the particle velocities, and the propagation of the electrons and ions to new positions.
(3) Save the ion number reaching the emitter surface and save the total energy delivered by these ions to the emitter (these ions cause the secondary electron emission from the emitter).
(4) Remove particles reaching the cathode and anode surface and boundaries of the simulation region. The model does not consider electrons reaching the emitter surface, assuming that these high have no effect on the HC operation. Indeed, the results of simulations showed that the flux of these electrons is much smaller than the flux of emitted electrons, since only high-energy electrons ($\varepsilon_e > 30$ eV) can penetrate the cathode sheath.
(5) Calculate the electron-neutral (e–n) and ion-neutral (i–n) collisions. The e-n collisions are calculated using the null-collision event method[33] and i-n collisions using the method described in Ref. 34.
(6) Secondary electron emission (SEE) with the coefficient of secondary emission is defined as[13]

$$k_{\text{sec}} = 0.01 + 3 \times 10^{-5} \cdot \varepsilon_{ion}^{1.455}. \quad (2)$$

Here ε_{ion} is the energy of the incident ion.
(7) Back to step #1.

Let us note that the heating of the HC by the plasma ions and heat transfer processes were not considered in the present model, and these issues will be considered in our upcoming research.

In the model, neutrals are considered as a background with a uniform density distribution inside the HC and non-uniform distribution outside the HC. The *Xe* gas density outside of the HC is calculated as following. Neutral flux through the orifice is

$$\Phi_n = nvS, \quad (3)$$

where n is the neutral density at the orifice output, S is the cross-sectional area of the orifice, and v is the neutrals velocity. It was assumed that the gas velocity v is constant, and the gas uniformly expands from the orifice in 2π solid angle. Thus, inside the cathode-anode gap the neutral density at surface of the sphere with radius r can be estimated as

$$n(r) = \frac{nS}{2\pi r^2}. \quad (4)$$

Depending on the cathode potential and gas density numerical grid sizes dx and dy, time step and weight (i.e., the number of actual particles in one super-particle) of super-particles pw were varied. For instance, at $\varphi_C = -100$ V and gas pressure inside HC of 150 Torr, $dx = 1.6 \times 10^{-6}$ m, $dy = 3.55 \times 10^{-6}$ m, $dt = 10^{-13}$ s, $pw = 10^7$. In the simulations, the total number of super-particles was varied in the range of 10^5–10^6. The time step is mainly controlled by the requirement to have $< 10\%$ of collisions each time step, since the Courant condition[35] $dx/V_{\max} < dt$ is satisfied at the given conditions. Here, $V_{\max}$ is the largest electron velocity obtained at given value of φ_C, i.e., $V_{\max} = \sqrt{2q_e|\varphi_C|/m_e}$, where q_e and m_e are the charge and mass of electron, respectively. If the gas pressure increases, one needs to decrease the time step. Also, the convergence analysis showed that an increase in φ_C requires a decrease in the space step.

A. Electron-neutral collisions

The e-n collisions are studied following the null-collision event method described in Ref. 33. Since electrons are more mobile than the neutrals, the neutrals are assumed unmovable, when the collision probability is calculated. According to the null-collision method (see Fig. 2) during each time step, the total number of electrons colliding with neutrals is calculated. This number is defined by the maximum collision frequency and gas density. The maximum collision frequency corresponds to the maximum value of the sum of collision cross sections (see Fig. 2). In the present model, elastic scattering, excitation, ionization, recombination, and null collisions (i.e., the collisions which do not lead to the change in the energy or momentum of electrons) have been considered

$$\nu_{\max} = \max(n_g) \cdot \max(\sigma_{total} \cdot V_{\max}). \quad (5)$$

Here, $\max(n_g)$ is the maximal gas density, which is realized inside the HC, and $V_{\max}$ is the electron velocity corresponding to maximum of collisional cross-section (see Fig. 2). Then, the fraction of colliding electrons during each time step is

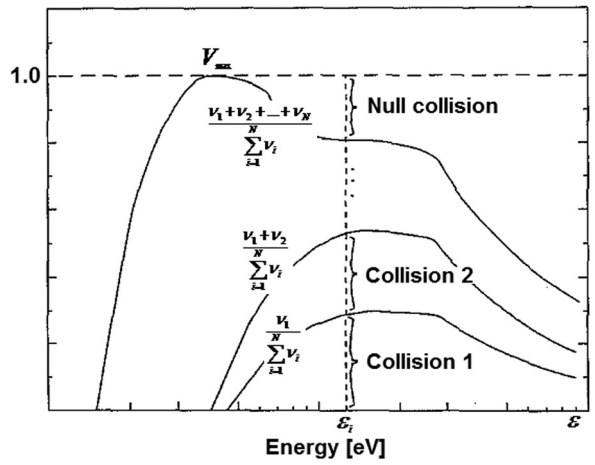

FIG. 2. The addition of the null collision process results in a constant collision frequency over all energies (see Ref. 33). Here, ν_i is the frequency of elastic scattering, excitation, ionization, and recombination collisions.

$$P_{coll} = 1 - \exp(\nu_{\max} dt). \tag{6}$$

Thus, each time step, the number of electrons $N_e \times P_{coll}$ which experience collisions with neutrals, is chosen randomly from the N_e electrons in the simulation domain.

In order to define the type of collision, a random number in the interval (0;1) is generated and is compared with the collision cross sections that are normalized following the method described in Ref. 33 and shown in Fig. 2. When the collision type is defined, the components of electron velocity after this collision are calculated. The angle of the electron trajectory before scattering event

$$\cos\vartheta = v_x/v,$$

where v is the absolute electron velocity. Isotropic scattering is assumed in calculating the angle after collision. Namely, a new random number r_1 from the interval (0;1) is generated and the scattering angle is calculated as

$$\cos\chi = 1 - 2 \cdot r_1. \tag{7}$$

The isotropic scattering model describes correctly the collision process between electrons and neutrals, when the energy of electrons does not exceed 1 keV, which is the case in our simulations. Then, the unit vectors in the direction of velocity after the scattering are[36]

$$e_x = \cos\vartheta \cdot \cos\chi - \sin\chi \cdot \sin\vartheta, \tag{8a}$$

$$e_y = \sin\vartheta \cdot \cos\chi + \sin\chi \cdot \cos\vartheta. \tag{8b}$$

The electron energy losses depend on the type of collision. If elastic scattering occurs, the energy losses are determined as

$$\Delta\varepsilon_{el} = 2m_e/M \cdot (1 - \cos\chi) \cdot \varepsilon. \tag{9}$$

Here, M is the atom mass, and ε is the electron energy before collision. If excitation occurs, the energy losses are equal to the excitation energy of atom (for *Xe*, the excitation energy is of 8.4 eV). If ionization occurs, the energy of new generated electron is defined as[33]

$$\varepsilon_{ej} = B \cdot \tan(r_2 \cdot \arctan((\varepsilon - I)/2B)), \tag{10}$$

where $B = 10$ eV, r_2 is the random number in the interval (0;1), and I is the ionization energy ($I = 12.1$ eV for *Xe* atoms). Then, the energy loss of the primary electron is

$$\Delta\varepsilon_i = \varepsilon - \varepsilon_{ej} - I. \tag{11}$$

The propagation angle of the electron generated after ionization is defined by Eq. (7) with a new random number in the interval (0;1). The velocity of the generated ion is chosen randomly from the Maxwellian distribution characterized by the temperature corresponding to the gas temperature.

If the type of electron collision is recombination, the closest ion which recombines with this electron is found and these electron and ion are then removed from the simulation. This closest ion is chosen randomly from the ions present in the space with the size $dx \times dy$ with the recombined electron in the center.

Here, let us note that the Coulomb electron-ion collisions were not considered in the present model. As will be shown further, the largest ionization degree is obtained inside the orifice and it is $\alpha \sim 10^{-3}$, where the gas pressure is of 150 Torr. An average energy of electrons in this location is of ~2 eV. The elastic scattering cross section for electrons with energy of 2 eV is $\sigma_{el} \sim 8 \times 10^{-16}$ cm^2, while the cross section of Coulomb collisions is $\sigma_C \sim 6 \times 10^{-14}$ cm^2,[31] i.e., $\sigma_{el}/\sigma_C \gg \alpha$ and, therefore, one can neglect by Coulomb collisions.

B. Ion-neutral collisions

For the considered gas temperatures, the velocities of neutrals become non-negligible compared to the ion velocities. Therefore, one cannot neglect the neutral velocity in comparison with the ion velocity, when the collision probability is calculated. Elastic scattering and charge-exchange ion-neutral collisions are considered in the model. The cross section of charge-exchange collision is calculated as[37]

$$\sigma_{CE} = (k_1 \cdot \ln|V_{ion} - V_n| + k_2)^2 \times 10^{-20}\,[m^2]. \tag{12}$$

Here, $k_1 = -0.8821$ and $k_2 = 15.1262$ are the constants, V_{ion} is the ion velocity, and V_n is the neutral velocity chosen randomly from the Maxwellian distribution with the temperature T_g. The elastic scattering cross section is defined as[38]

$$\sigma_{EL} = 6.42 \times 10^{-16}/|V_{ion} - V_n|\,[m^2] \tag{13}$$

and the probability for each ion to experience collision with neutral

$$P = 1 - \exp(|V_{ion} - V_n| dt_{ion}/\lambda), \tag{14}$$

where dt_{ion} is the time step used for ion-neutral collision, and λ is the ion mean free path in the neutral gas. Here, let us note that the time step dt_{ion} is selected to satisfy condition $P \le 0.1$, which means that the ion propagates only a small fraction of its mean free path during dt_{ion}. Note that step dt_{ion} is significantly larger than the time step dt used for calculation of electron motion.

When the values of probability P are calculated, a set of random numbers between 0 and 1 is generated and compared with P. If P exceeds the random number, a collision occurs. The isotropic scattering model is assumed and the scattering angle is calculated following the method described in Ref. 34. If the elastic scattering occurs, the ion and neutral velocity components are calculated as

$$v'_{ix} = \frac{1}{2}(v_{ix} + v_{nx} + |v_i - v_n| \cdot \cos\chi),$$

$$v'_{iy} = \frac{1}{2}(v_{iy} + v_{ny} + |v_i - v_n| \cdot \sin\chi),$$

$$v'_{nx} = \frac{1}{2}(v_{ix} + v_{nx} - |v_i - v_n| \cdot \cos\chi),$$

$$v'_{ny} = \frac{1}{2}(v_{iy} + v_{ny} - |v_i - v_n| \cdot \sin\chi).$$

Here, $|v_i - v_n| = \sqrt{(v_{ix} - v_{nx})^2 + (v_{iy} - v_{ny})^2}$ is the relative ion-neutral velocity. If the charge-exchange collision occurs $v'_{ix} = v'_{nx}$, $v'_{iy} = v'_{ny}$, $v'_{nx} = v'_{ix}$, and $v'_{ny} = v'_{iy}$. For a detailed description of the model used for calculation of ion-neutral collisions, see Ref. 34.

III. RESULTS AND DISCUSSION

A. Breakdown stage of the HC operation

Fig. 1 shows the geometry of the orificed HC studied in the present work. The inner and outer transverse and longitudinal lengths of the HC are of 0.2 mm, 0.75 mm, and 2 mm, respectively, and the cathode-anode distance is of 2 mm. The potential of the cathode is considered to be a constant $\varphi_C = -100$ V and the work function of the cathode material is of 1.5 eV. The temperature of the cathode $T_C = 1500$ K, which is considered to be equal to the *Xe* gas temperature T and the gas pressure is $P = 150$ Torr. The front of the cathode is covered by the conducting plate with potential equal to the cathode, i.e., emitter potential. The plate has a central orifice with width of 0.1 mm and length of 0.05 mm.

In order to decrease the computation time in the simulations, all the dimensions were decreased by 10 times. The value of the electric field E and ratio E/P, which determine type of electron collisions were kept as in actual geometry. In addition, the HC length was decreased two times and the mass of the *Xe* atoms was decreased 100 times, in order to reach the steady state faster. Several test simulations which included different HC dimensions showed that these changes do not influence the steady state parameters of the HC operation. In addition, several test simulations were carried out with different time and space cells to demonstrate convergence of the simulations to steady state conditions, i.e., when the parameters of the plasma and potential distribution reach steady state.

The evolution of the potential and electron and ion distributions, during the gas discharge, is shown in Figs. 3–5. The simulation results show that the breakdown occurs in several stages. At the beginning of the discharge initiation, the potential inside the HC is constant and equal to the cathode potential. Thus, the electric field inside the HC is zero and electrons emitted from the emitter due to thermionic emission do not ionize the gas. Velocity of these electrons is small and they cannot rapidly escape the HC. Space charge of these electrons shields thermionic emission from the emitter except very narrow section near the orifice. Electrons, which leave the HC through the orifice, gain energy, due to acceleration in the applied electric field, sufficient to ionize *Xe* atoms. Since the density of the *Xe* gas is non-uniform outside the HC, the ionization rate decreases towards the anode. The generated ions start to propagate towards the orifice. A part of these ions is lost at the orifice plate and a part of the ions penetrates inside HC. Since the density of the generated plasma is small, the potential distribution inside and outside the HC does not changed noticeably during this stage.

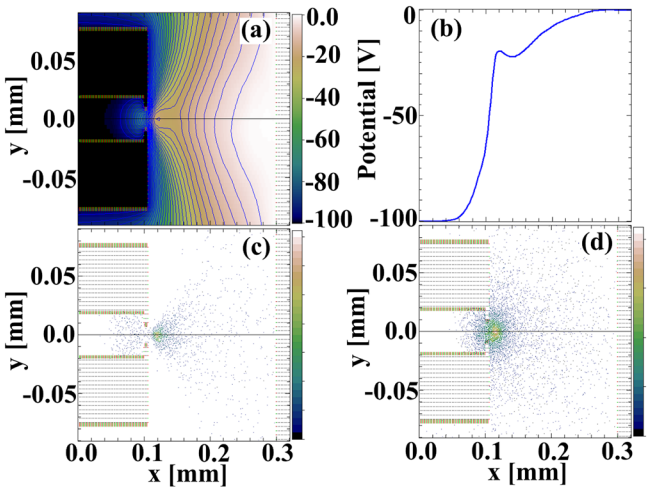

FIG. 3. (a) 2D potential distribution; (b) potential distribution along the system axis; (c) electron distribution; (d) ion distribution. $t = 89$ ns.

During the second stage of the discharge (see Fig. 3), the plasma density in the orifice reaches $n_e \sim 6 \times 10^{20}$ m^{-3} and the potential inside the orifice and HC starts to be disturbed. Fig. 3(a) shows that a positive potential well with respect to the HC wall appears inside the HC. Beginning

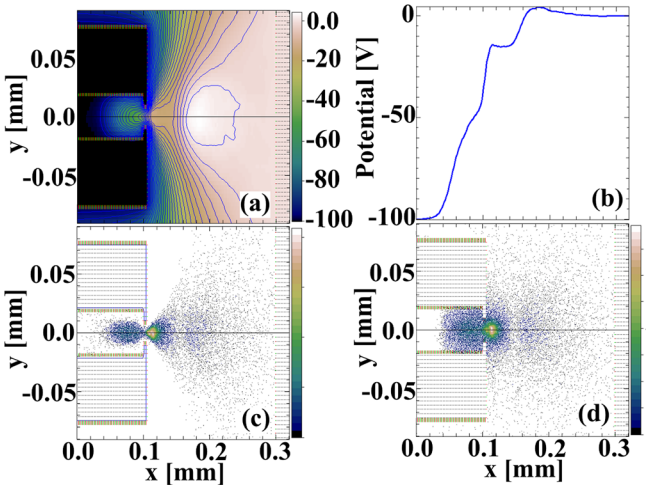

FIG. 4. (a) 2D potential distribution; (b) potential distribution at the system axis; (c) electron distribution; and (d) ion distribution. $t = 92.5$ ns.

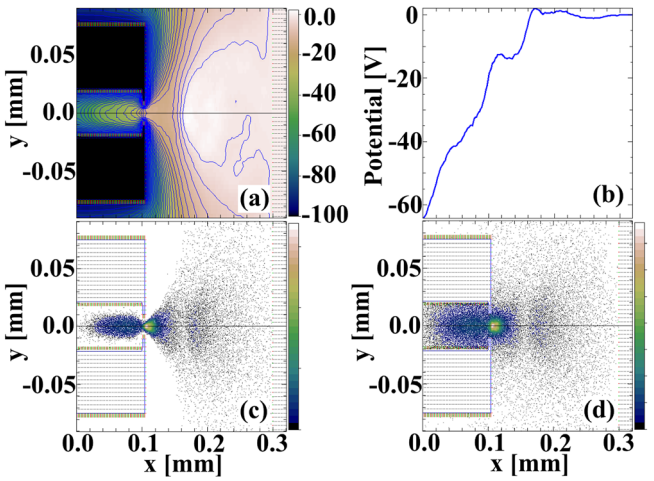

FIG. 5. (a) 2D potential distribution; (b) potential distribution at the system axis; (c) electron distribution; (d) ion distribution. $t = 96$ ns.

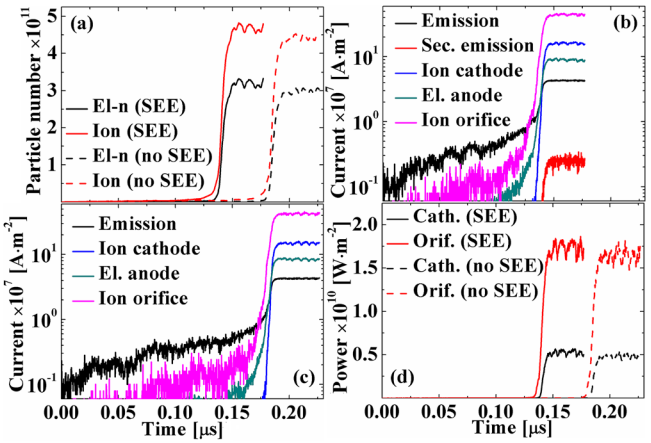

FIG. 6. (a) Electron and ion number in the system in the model with and without SEE; (b) electron and ion current densities in the model with SEE; (c) electron and ion current in the model without SEE; (d) comparison between powers delivered to the emitter and to the orifice in the models with and without SEE.

$t \approx 80$ ns, the depth of this well exceeds the ionization potential of *Xe* atoms and plasma starts to be generated also inside the HC. The potential distribution along the central axis at $t = 89$ ns demonstrates [see Fig. 3(b)], the appearance of the region ($0.011\,\text{mm} < x < 0.012\,\text{mm}$) of uncompensated negative/positive charge outside the HC, which is caused by different mobility of electrons and ions. The appearance of this region which can be identified as a double sheath, leads to shortening of the distance, where electrons acquire energy $\varepsilon_e > I$, and, increases in the rate of the plasma generation at that location. Also, ions acquire significant directed velocities towards the orifice plate as a result of being accelerated in this double layer.

During the third stage (see Figs. 4 and 5), the plasma density inside orifice reaches $n_e \sim 1.5 \times 10^{21}\,\text{m}^{-3}$ and the plasma is generated efficiently from the both sides of the orifice. On the one hand, the front of the plasma with positive potential with respect to the HC wall propagates towards the left boundary of the HC. Electrons emitted by the emitter due to either thermionic or secondary emission oscillate in this potential well, creating new electron-ion pairs and increasing the plasma density inside the HC. Inside the cathode-anode gap, acceleration of ions occurs mainly in the double layer formed between the plasma acquiring almost the anode potential and the dense plasma (cathode plume) formed in the vicinity of the output of the orifice.

B. Steady state phase of the HC operation

The results of simulations showed that for the given parameters, the steady state operation of the HC is reached at $t \approx 0.12\,\mu$s. At $P = 150$ Torr and $\varphi_C = -100$ V, the plasma density inside the orifice is not changed as compared with the density obtained in the third stage of the discharge, i.e., $n_e \sim 1.5 \times 10^{21}\,\text{m}^{-3}$, but the density of the plasma inside the HC increases reaching $n_e \sim 1.0 \times 10^{20}\,\text{m}^{-3}$. The total actual number of electrons and ions present in the system is shown in Fig. 6. One can see that the number of ions exceeds the number of electrons, which is due to the larger electron mobility in comparison with the ion mobility. Thus, electrons escape the simulation domain faster than the ions, which also explain positive potential of the plasma. For comparison, additional simulations were carried out without including SEE. The results of these simulations showed that for the considered coefficient of SEE, the steady state is reached later, although the number of particles in the system is not changed significantly. The latter indicates the minor role of SEE on steady state parameters of the HC operation at the given conditions as it was found also in simulations of much larger cathodes used in electric propulsion.[4,23]

The comparisons between electron current densities, obtained in the simulations with and without SEE, emitted by the emitter and reaching the anode are shown in Figs. 6(b) and 6(c), respectively. In these figures, the ion current densities towards the emitter are also presented. One can see that SEE current density is almost 15 times smaller than the current density of thermionic electrons, which explains the insignificant difference in the total electron and ion numbers and current densities shown in Figs. 6(a)–6(c). The largest current density is obtained for ion flow towards the orifice walls, which is explained by the increased plasma density in this location [see Figs. 5(c) and 5(d)]. Also, as will be shown below, the ions acquire maximal radial velocity inside the HC in the vicinity of the orifice, where one obtains the largest depth of the potential well. Here, let us note that without accounting for the Schottky effect, Richardson's law gives electron current density of $J_e \approx 2.5 \times 10^7\,\text{A·m}^{-2}$, while Fig. 6(b) shows that in steady state $J_e \approx 4.5 \times 10^7\,\text{A·m}^{-2}$. This indicates that the presence of ions inside the HC increases the electric field at the emitter surface, resulting in the increase of electron thermionic emission. The steady state electron current reaching the anode at the given conditions is ~20 A.

Comparison between power densities delivered by ions to the HC emitter, W_c, and orifice walls, W_{or} shows [see Fig. 6(d)] that $W_{or}/W_c \sim 3$. This is explained by the greater ion energy near the orifice than ion energy inside the HC and this should lead to non-uniform heating and erosion of the emitter. Let us estimate the average rate of emitter erosion $\Delta h/\Delta t$ following the method, presented in Ref. 28. If erosion

occurs as a result of surface sputtering by Xe^+ ion bombardment, the sputtering yield for tungsten as a function of ion energy ε_i is

$$Y(\varepsilon_i) = \exp\{-38.744 \cdot [4.3429 \cdot \ln(\varepsilon_i) - 9]^{-0.5} + 8.101\}.$$

When ions collide with the a cylindrical emitter having the length l_C and inner radius R_C, the number of atoms sputtered off the inner surface of the cathode in a given time interval Δt is $2\pi R_C \cdot l_C \cdot (n_i u_i) \cdot Y(\varepsilon_i) \cdot \Delta t$, where $(n_i u_i)$ is the ion flux towards the emitter. The number of atoms in an element of volume is $\frac{\rho N_A}{A_w} l_C \pi(\Delta h^2 + 2R_C \Delta h)$, where $\rho = 19.25 \times 10^3\,\mathrm{kg \cdot m^{-3}}$ is the tungsten density, $N_A = 6 \times 10^{23}\,\mathrm{mol^{-1}}$ is the Avogadro's number, $A_w = 0.183\,\mathrm{kg \cdot mol^{-1}}$ is the atomic weight of tungsten. Thus, the average rate of emitter erosion reads

$$\Delta h/\Delta t = R_C/\Delta t \cdot \left(\sqrt{1 + \frac{2\Delta t}{R_C}\frac{A_w}{\rho N_A}(n_i u_i)Y} - 1\right).$$

The results of simulations showed that the average energy of ions energy interacting with the emitter is $\varepsilon_i \approx 15\,\mathrm{eV}$ that results in the value of sputtering yield $Y(15\,\mathrm{eV}) \approx 2.5 \times 10^{-7}$. Taking into account that $R_C = 0.2\,\mathrm{mm}$ and assuming $\Delta t = 220\,\mathrm{h}$, one obtains the average erosion rate $\Delta h/\Delta t \approx 0.94\,\mu\mathrm{m \cdot h^{-1}}$, which exceeds ~2.3 times the erosion rate obtained by Mikellides *et al.*[28] for larger HC.

Also, one can see that the emitter cooling due to power density of thermionic electrons $\varepsilon_{th} \approx 4.3 \times 10^7\,\mathrm{Wm^{-2}}$ and secondary electrons $\varepsilon_{SEE} \approx 0.3 \times 10^7\,\mathrm{W/m^2}$ can be considered as negligible compared with the power density delivered by ions to the emitter. It is important to note that these results are in partial agreement with the results presented in Ref. 24, where two different HCs were studied. In that, numerical research was obtained that the heating and cooling of the HC is mainly due to the electron flux toward and outward the emitter, when the emitter inner diameter was 0.635 cm and the orifice diameter was 0.1 cm. The opposite effect was obtained for the HC with the emitter inner diameter of 1.5 cm and the orifice diameter of 0.3 cm, i.e., the emitter heating was mainly due to the ion bombardment. However, the fluxes of emitted and absorbed electrons were comparable with the ion flux. The difference in heating mechanisms was explained by larger potential of the plasma in the case of the larger cathode which results in larger sheath potential, and, respectively, in larger energy of ions which interact with the emitter and smaller flux of plasma electrons towards the emitter.

The potential, number of particles, radial and axial profiles of electron and ion density, electron and ion energy distribution, and particle phase distributions in the steady state mode of the HC operation, are shown in Figs. 7–12. One can see that the HC discharge can be separated into several regions (see, Figs. 7–10), which agree with the results obtained, for instance, by Mikellides *et al.*[22–30] The 1st region, $0 < x < 0.1\,\mathrm{mm}$ is located inside the HC and is characterized by plasma density increasing towards the orifice plate. The 2nd region, $0.1\,\mathrm{mm} < x < 0.12\,\mathrm{mm}$, is related to

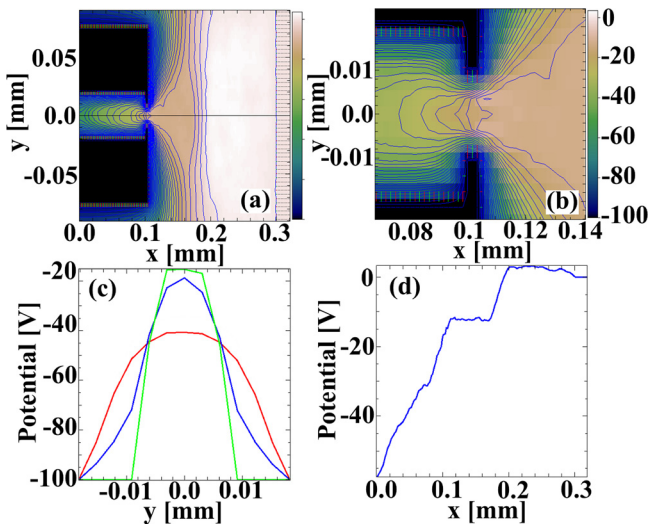

FIG. 7. (a) 2D potential distribution. (b) Zoomed 2D potential distribution at the region of the orifice plate. (c) Radial potential distribution at the entrance ($x = 0.1\,\mathrm{mm}$) of the HC (blue line), in the middle of the HC (red line, $x = 0.05\,\mathrm{mm}$), and inside the orifice plate (green line). (d) Axial potential distribution.

the plasma inside the orifice, where one obtains the largest plasma density. The 3rd region, $0.12\,\mathrm{mm} < x < 0.165\,\mathrm{mm}$, is the cathode plasma plume which occupies significant space inside the cathode-anode gap. The 4th region, $0.175\,\mathrm{mm} < x < 0.27$ is occupied by the plasma having slightly positive (<2 V) potential. Between the cathode plasma plume and this slightly positive charged plasma, one obtains a double sheath with potential difference of ~12 V. Finally, 5th region, $0.27\,\mathrm{mm} < x < 0.3\,\mathrm{mm}$, is the anode sheath with plasma potential ≤2 V. It was found that the value of positive plasma potential depends on the gas pressure and cathode potential. Namely, an increase in the value of φ_C and pressure leads to the decrease and disappearance of this potential of the plasma.

The axial distribution of the plasma potential inside the orifice shows that its value remains constant, i.e., axial

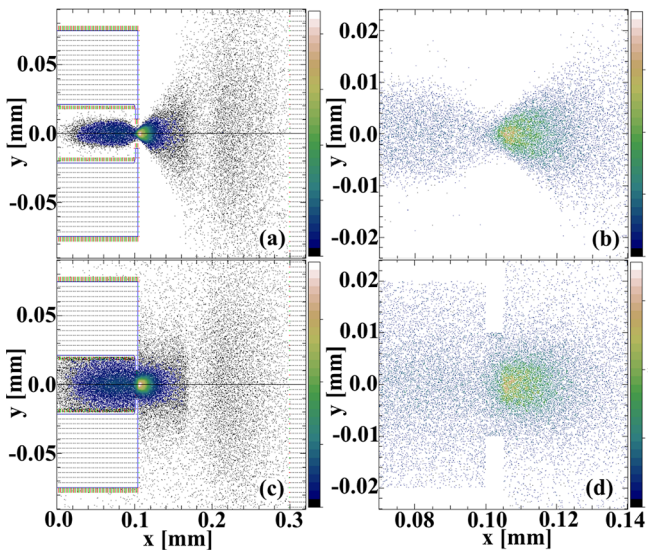

FIG. 8. Distributions of electron (a) and (b) and ion (c) and (d) particles in the steady state mode of the HC operation.

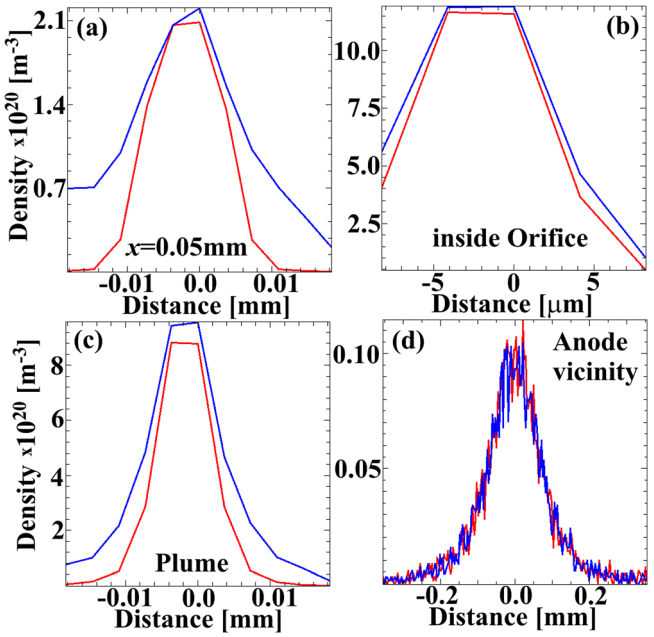

FIG. 9. Transversal profile of electron (red line) and ion (blue line) density at different positions along x-axis.

component of the electric field is almost zero, which indicates a sufficient average electron energy and plasma density resulting in an increase in the plasma conductivity in that region. Inside the HC, one obtains both axial and radial dependencies of the potential distribution. The radial distribution of the potential (potential well) is characterized by its maximum value at the axis, which depends on coordinate x and increases towards the orifice. Thus, some of the ions reaching the HC walls acquire energy up to 90 eV, which can cause significant sputtering of the cathode. Thermionic and secondary electrons emitted from the emitter and accelerated in the cathode sheath (the gap between the cathode wall and the plasma, where the electric field is almost zero) gain energy sufficient to ionize gas. At *Xe* gas pressure of 150 Torr, the electron mean free path is $\lambda \sim 3 \times 10^{-6}$ m, which is much smaller than the inner cathode radius. Thus, the effect of electron pendulum motion in the potential well formed by positively charged plasma is not important at the considered conditions, and the HC discharge is supported by electrons emitted from the emitter and accelerated in the cathode sheath. Also, the electron mean free path is smaller than the cathode sheath length l_{sh} near the orifice, where

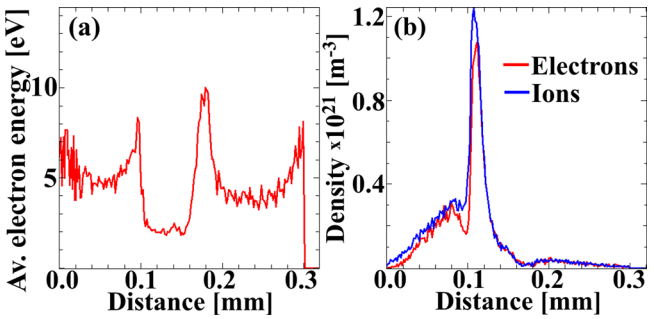

FIG. 10. (a) Spatial profile of the average electron energy; (b) axial profiles of electron and ion densities ($y = 0$).

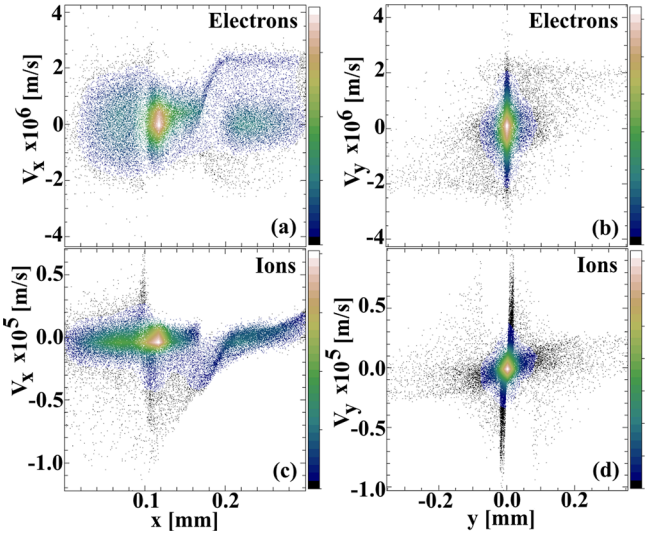

FIG. 11. Electron (a) and (b) and ion (c) and (d) phase space in the steady state of the HC operation.

$l_{sh} \sim 1.5 \times 10^{-5}$ m. Thus, the cathode sheath cannot be considered as collisionless at that location and electrons generated in this sheath also contribute to the plasma generation. The width of the cathode sheath decreases towards the left boundary and becomes $l_{sh} < 10^{-5}$ m [see Fig. 7(c)] at $x < 0.05$ mm. Thus, at those locations the ionization of *Xe* atoms inside the sheath becomes insignificant.

Figs. 8–10(b) show that the largest plasma density is realized in the vicinity of the output of the orifice, namely, its value at 0.1 mm $< x <$ 0.12 mm exceeds the plasma density inside the cathode more than the order of magnitude. The regions with dilute plasma one obtains in the vicinity of the cathode walls, between the cathode plume and the slightly positively charged plasma and in the vicinity of the

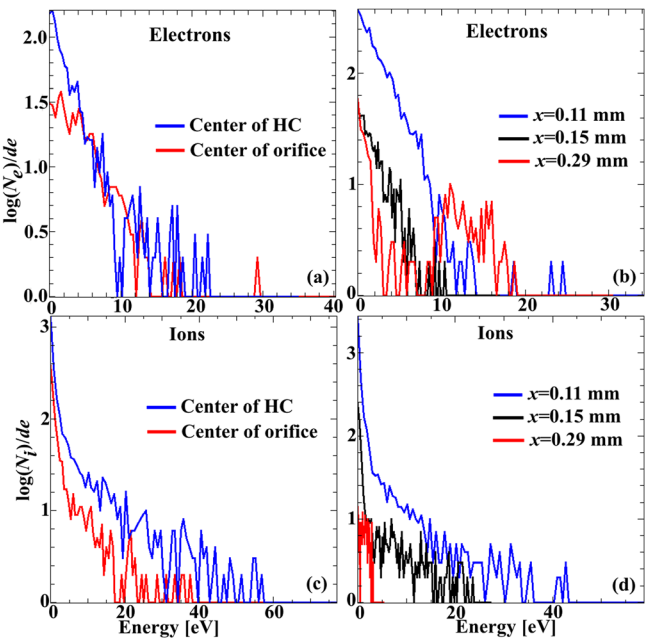

FIG. 12. Electron (a) and (b) and ion (c) and (d) energy distribution functions in the steady state of the HC operation obtained at different axial planes.

anode. The particle distribution [see Fig. 10(b)] shows that the plasma density inside the HC decreases versus the distance from the orifice, being the smallest at the HC left boundary. It is caused by the electron scattering, which leads to the escape of electrons from the simulation domain.

The transverse (along the Y-axis) density distribution of plasma particles at different positions along X-axis (see Fig. 9) shows that the largest plasma density is realized at $y = 0$. A quasi-constant density of the plasma electrons and ions occurs only in the narrow region with width of a few microns inside the orifice and $\sim 200\,\mu$m inside the HC; further, the density of plasma particles decreases rather rapidly with the distance from the Y-axis, showing formation of plasma sheaths in the vicinity of the HC and orifice walls.

Distribution of average electron energy along X-axis is shown in Fig. 10(a). The average electron energy was calculated as

$$\bar{\varepsilon}(x) = \frac{\int \varepsilon \cdot f(\varepsilon, x) d\varepsilon}{\int f(\varepsilon, x) d\varepsilon},$$

where $f(\varepsilon, x)$ is the electron energy distribution function averaged along Y-axis for certain x coordinate [see, for instance, Figs. 12(a) and 12(b)]. The smallest value of $\bar{\varepsilon} \approx 2\,$eV is obtained in the vicinity of the orifice, where the largest density of plasma is realized [see Fig. 10(b)]. Inside the HC and in the vicinity of the anode, the plasma density is much smaller than in the orifice and the larger $\bar{\varepsilon}$ is obtained. The largest averaged electron energy is the region of the double layer (up to 10 eV), inside the HC in the vicinity of the orifice plate, where the potential difference between the plasma and emitter reaches its maximum, and close to the anode.

The electron velocity phase space [see, Figs. 11(a) and 11(b)] and electron energy distribution function [see Figs. 12(a) and 12(b)] show an electron beam, which is generated in the double sheath formed between the cathode plasma plume and the slightly positive anode plasma. One can see that electrons acquire energies up to 20 eV, which agrees with the energy spectrum of electrons measured behind the anode in experiments described in Ref. 22. These energetic electrons propagate towards the anode almost collisionless because in neutrals ($n_n \leq 5 \times 10^{23}\,\mathrm{m}^{-3}$) and plasma ($n_{pl} \leq 10^{19}\,\mathrm{m}^{-3}$), the mean free path of these electrons is significantly larger than the propagation distance. In the cathode plasma plume and the slightly positively charged anode plasma, the main part of electrons can be characterized by a Maxwellian velocity distribution with mean energy of $\sim 2\,$eV [see Figs. 10(a) and 12(b)]. However, one can find rather energetic electrons at the tail of this velocity distribution. Inside the HC plasma, the electron velocity distribution is rather broad because of oscillating electrons and it can be characterized by a mean energy of electrons of $\sim 5\,$eV [see Figs. 10(a) and 12(a)].

The ion velocity phase space is shown in Figs. 11(c) and 11(d) and the ion energy distribution functions at different locations along x-axis are shown in Figs. 12(c) and 12(d). Here, one can see that ions acquire energy up to 20 eV in the double layer. However, the main part of these energetic ions does not reach the orifice plate because of the large charge-exchange cross section and, small mean free path ($<10\,\mu$m). Another region where ions acquire large energy is inside the HC near the orifice, where one obtains the largest radial potential difference between the plasma and the HC walls. Let us note here that the simulations show, at the exit of the orifice, a flux of ions with velocities directed outside the HC. However, the axial potential distribution allows acceleration of ions only along x-axis inward the HC. Also, ions are generated from neutrals, which have a Maxwellian velocity distribution. Thus, the flux of ions outward the cathode is formed by ion-neutral elastic collisions, which are the most frequent at that location due to the large neutral density. The ion velocity distribution function inside the HC cannot be considered as Maxwellian [see Figs. 11(c) and 12(c)].

In Table I, we present results of additional simulations, which were carried out in order to show the influence of gas pressure, cathode potential, and orifice size on the steady state parameters of the HC operation. The last row in Table I contains parameters obtained for the HC without an orifice, with the same geometry as the orificed HC. One can see that an increase in pressure of *Xe* gas, while keeping all other initial parameters unchanged, leads to an almost linear decrease in the power delivered by ion flow to the cathode and orifice walls. This occurs due to an increase in the plasma density inside the cathode and a decrease in the potential difference between the plasma and the emitter walls. Also, it was found that the increase in pressure causes a decrease in the radius of the cathode plasma plume and in the width of the sheath between the plasma and cathode walls. The decrease in the sheath width decreases the number of electrons which are generated inside the sheath and leads to a smaller electron number oscillating in the potential well and generating new electron-ion pairs. The decrease in the potential difference also leads to a decreases number of emitted electrons and to a decrease of the plasma density inside the HC.

Opposite to the effect of the increase in the pressure, the increase in the cathode potential leads to drastic increase in ion flow and, respectively, the energy, delivered to the cathode and orifice walls. At the earlier stage of the discharge, the increase in φ_C does not significantly influence the electron thermionic since $E_C(x) \approx 0$ due to the electric field shielding inside the HC. However, the increase in cathode potential φ_C results in the decrease in the distance outside the HC, where electrons acquire the energy sufficient to ionize the gas. This leads to faster formation of the plasma at that location and to increase in the ion flux, which penetrates inside the HC. As a consequence, positively charged plasma appears inside the HC, which causes the increase in the electric field at the cathode surface E_C. The latter increases the thermionic electron emission due to Schottky effect. The Richardson-Dushman law [Eq. (1)] dictates that an increase in E_C leads to the increase in emitted electron current density. This leads to significant increase in the electron flux outside the orifice that increases the rate of the plasma generation. As a consequence, the ion flux inside the HC increases, the plasma density in the vicinity of the orifice

TABLE I. Influence of gas pressure, cathode potential, and orifice radius on the steady state parameters of the HC operation.

φ_C; r_{of}; P	Therm. el-ns, 10^7 A·m^{-2}	W_e, 10^7 W·m^{-2}	SEE, 10^7 A·m^{-2}	Ion cath., 10^7 A·m^{-2}	W_i, 10^7 W·m^{-2}	El. anode, 10^7 A·m^{-2}	Ion orif., 10^7 A·m^{-2}	W_{ior}, 10^7 W·m^{-2}	n_{emax}, 10^{21} m^{-3}
−100 V; 0.1 mm; 100 Torr	4.54	1.2	0.7	20.1	766	12.0	58.0	2724	0.9
−100 V; 0.1 mm; 150 Torr	4.28	1.0	0.3	15.5	500	8.8	45.1	1712	1.4
−100 V; 0.1 mm; 200 Torr	4.25	1.0	0.3	12.8	279	7.9	38.4	1240	2.0
−150 V; 0.1 mm; 100 Torr	5.5	1.5	1.8	58.9	4924	33.4	178.2	1.5×10^4	2.3
−200 V; 0.1 mm; 100 Torr	6.3	1.9	3.0	100.1	2053	50.6	340.1	2.1×10^5	4.0
−150 V; 0.09 mm; 100 Torr	5.21	1.4	1.1	42.4	2861	24.1	133.8	9756	2.1
−150 V; 0.11 mm; 100 Torr	5.62	1.6	1.6	55.4	4374	26.4	106.3	8500	2.5
−150 V; 0.2 mm; 100 Torr	5.7	1.6	1.5	53.1	4118	20.0	…	…	1.8

also increases, and the steady state is reached faster. The increase in current of emitted electrons results in the increase in the electron flux through the anode, i.e., the increase in cathode potential leads to the increase in discharge current (see Table I). Similar dependence of discharge current on discharge voltage was obtained in Ref. 4 for high operating currents.

It was found that parameters of the orificed HC discharge are non-monotonic functions of the orifice transverse size (which can be called radius) r_{or}, i.e., there is some optimal r_{or}, which allows generation of currents comparable to the case of the operation of the HC without orifice. Simulations showed that when r_{or} is smaller than this optimal value, the HC discharge is not initiated since the main part of thermionic emitted electrons is lost in the orifice. The number of electrons passing through the orifice does not allow one to generate dense plasma outside the HC, and the ion flux towards the HC is not sufficient to initiate the HC effect. Also, it was found that the increase in the value of r_{or} leads to a decrease in the time, when the steady state mode of the HC operation is reached. This is explained by the increasing flux of electrons outside the orifice, which increases the rate of plasma generation and, respectively, increases the ion flux towards the HC. Table I shows that the increase in the orifice radius results in the increase in the plasma peak density. This result disagrees with the fluid simulation results, presented in Ref. 27, where the opposite tendency was obtained. However, it is important to note that Katz *et al.*[27] studied three different regimes of HC, namely, when the ratio between orifice radius and length changes drastically. In the present paper, we studied the regime, when the orifice radius exceeds its length. This regime corresponds to the Type B of HC, considered in Ref. 27.

Finally, Table I shows that the largest ion flux is obtained on the orifice plate independently on the conditions, considered in our simulations. This result agrees with the fluid simulations results for HC of Type B.[27] However, the ratio between ion fluxes to the orifice and to the emitter is much larger for the conditions considered in the present paper. This can be explained by much larger gas pressure, which results in the larger cathode sheath potential and, as a consequence, results in the larger ion energy bombarded the plates.

IV. SUMMARY

A self-consistent 2D PIC Monte Carlo collision model was developed and used for numerical simulation of the operation of the micro-hollow cathode with and without orifice and with a thermionic emitter for different values of *Xe* gas pressure, orifice size, and applied voltage. The model includes thermionic electron emission, SEE, electron-ion recombination, and electron-neutral different collision processes and non-uniform *Xe* gas density in the cathode-anode gap. The numerical simulations allow one to determine plasma particle density and energy at different locations of the HC, potential, axial and radial distribution, and energy flux towards the HC and orifice walls. Simulation showed formation inside the HC of a sheath between the plasma acquiring positive potential and the emitter with potential differences up to several tens of Volts. Also, a double sheath formation between the cathode plasma plume and the anode

plasma was obtained in these simulations. Electron acceleration in this double sheath leads to generation of an energetic electron flux towards the anode. The denser plasma was obtained in the vicinity of the output of the orifice.

In addition, the results of simulations which were carried out for different *Xe* gas pressure, orifice radius and cathode voltage on parameters of the micro-hollow cathode operation are presented and discussed. Carried out 2D PIC simulations of micro-HC operation in a diode geometry for a given equal temperature of the emitter and gas showed that the increase in gas pressure results in the decrease in the current density of thermo- and secondary emitted electrons, as well as in the decrease in both the ion current density to the cathode and to the orifice plate. The increase in the cathode potential leads to the faster formation inside the HC of the plasma, which acquires a positive potential leading to the increase in ion current densities towards the cathode and orifice and leads to the increase in thermo- and secondary emitted electron current densities. The simulations results showed significant deviation of the electron energy distribution changes along the emitter and deviates from Maxwellian energy distribution function. Also, it was shown that the energy of ions accelerating inside the cathode sheath can reach tens of eV which could lead to fast erosion of the emitter and orifice.

ACKNOWLEDGMENTS

This work was supported in part at the Technion by a fellowship from the Lady Davis Foundation.

[1]J. V. Sullivan and A. Walsh, Spectrochim. Acta **21**, 721 (1965).
[2]D. Mihailova, J. van Dijk, G. J. M. Hagelaar, S. Karatodorov, P. Zahariev, M. Grozeva, and J. J. A. M. van der Mullen, J. Phys. D: Appl. Phys. **45**, 165201 (2012).
[3]J. Hopwood, *Ionized Physical Vapor Deposition*, Thin Film Series Vol. 27 (Academic Press, San Diego, 2000).
[4]D. Goebel and I. Katz, *Fundamentals of Electric Propulsion* (John Wiley & Sons, 2008).
[5]M. Keidar, J. Appl. Phys. **103**, 053309 (2008).
[6]Y. Raitses, D. Staack, M. Keidar, and N. J. Fisch, Phys. Plasmas **12**, 057104 (2005).
[7]A. Fruchtman, Phys. Plasmas **10**, 2100 (2003).
[8]J.-P. Boeuf and L. Garrigues, J. Appl. Phys. **84**, 3541 (1998).
[9]N. N. Koshelev and A. V. Loyan, in *Proceedings of the 30th International Electric Propulsion Conference, Florence, Italy*, 17–20 September 2007.
[10]P. F. Little and A. von Engel, Proc. R. Soc. London, Ser. A **224**, 209 (1954).
[11]E. Oks, *Plasma Cathode Electron Sources* (Wiley-VCH, 2006).
[12]G. J. Kim, F. Iza, and J. K. Lee, J. Phys. D: Appl. Phys. **39**, 4386 (2006).
[13]S. S. Yang, S. M. Lee, F. Iza, and J. K. Lee, J. Phys. D: Appl. Phys. **39**, 2775 (2006).
[14]A. K. Malik, P. Montarde, and M. G. Haines, J. Phys. D: Appl. Phys. **33**, 2037 (2000).
[15]P. S. Kothnur and L. L. Raja, J. Appl. Phys. **97**, 043305 (2005).
[16]F. Crawford and S. Gabriel, in *Proceedings of the 33rd AIAA Fluid Dynamics Conference and Exhibit, Orlando, FL, 2003, AIAA 03-3580* (AIAA, Washington, DC, 2003).
[17]I. Katz, J. E. Polk, I. G. Mikellides, D. M. Goebel, and S. E. Hornbeck, in *Proceedings of the 29th International Electric Propulsion Conference, Princeton University*, 31 October–4 November 2005.
[18]I. Katz, J. R. Anderson, J. E. Polk, and J. R. Brophy, J. Propul. Power **19**, 595 (2003).
[19]I. D. Boyd and M. W. Crofton, J. Appl. Phys. **95**, 3285 (2004).
[20]J. Mizrahi, V. Vekselman, V. Gurovich, and Y. E. Krasik, J. Propul. Power **28**, 1134 (2012).
[21]V. Vekselman, Y. E. Krasik, S. Gleizer, V. T. Gurovich, A. Warshavsky, and L. Rabinovich, J. Propul. Power **29**, 475 (2013).
[22]I. G. Mikkelides, I. Katz, D. M. Goebel, and J. E. Polk, in *Proceedings of the 41st AIAA/ASME/SAE/ASEE Joint Propulsion Conference & Exhibit, Tucson, Arizona*, AIAA 2005–4234, 10–13 July 2005.
[23]I. G. Mikkelides, I. Katz, D. M. Goebel, and J. E. Polk, J. Appl. Phys. **98**, 113303 (2005).
[24]I. G. Mikellides, I. Katz, D. M. Goebel, J. E. Polk, and K. K. Jameson, Phys. Plasmas **13**, 063504 (2006).
[25]I. G. Mikkelides, I. Katz, D. M. Goebel, and K. K. Jameson, J. Appl. Phys. **101**, 063301 (2007).
[26]I. G. Mikkelides, I. Katz, D. M. Goebel, K. K. Jameson, and J. E. Polk, J. Propul. Power **24**, 866 (2008).
[27]I. Katz, I. G. Mikkelides, D. M. Goebel, and J. E. Polk, IEEE Trans. Plasma Sci. **36**, 2199 (2008).
[28]I. G. Mikellides and I. Katz, J. Propul. Power **24**, 855 (2008).
[29]I. G. Mikkelides, Phys. Plasmas **16**, 013501 (2009).
[30]I. G. Mikellides, D. M. Goebel, J. S. Snyder, I. Katz, and D. A. Herman, J. Appl. Phys. **108**, 113308 (2010).
[31]Y. P. Raizer, *Gas Discharge Physics* (Springer-Verlag, 1991).
[32]D. P. Grote, A. Friedman, J. L. Vay, and I. Haber, AIP Conf. Proc. **749**, 55 (2005).
[33]V. Vahedi and M. Surendra, Comput. Phys. Commun. **87**, 179 (1995).
[34]K. Nanbu, IEEE Trans. Plasma Sci. **28**, 971 (2000).
[35]C. K. Birdsall and A. B. Langdon, *Plasma Physics via Computer Simulation* (IoP Publishing, Bristol, 1991).
[36]Z. Donko, Plasma Sources Sci. Technol. **20**, 024001 (2011).
[37]D. Rapp and W. E. Francis, J. Chem. Phys. **37**, 2631 (1962).
[38]A. Dalgarno, M. R. C. McDowell, and A. Williams, Proc. R. Soc. **250**, 411 (1958).